

Experimental evolution in morbidostat reveals converging genomic trajectories on the path to triclosan resistance

Semen A. Leyn¹, Jaime E. Zlamal¹, Oleg V. Kurnasov¹, Xiaoqing Li¹, Marinela Elane¹, Lourdes Myjak¹, Mikolaj Godzik¹, Alban de Crecy², Fernando Garcia-Alcalde³, Martin Ebeling⁴ and Andrei L. Osterman^{1,*}

Abstract

Understanding the dynamics and mechanisms of acquired drug resistance across major classes of antibiotics and bacterial pathogens is of critical importance for the optimization of current anti-infective therapies and the development of novel ones. To systematically address this challenge, we developed a workflow combining experimental evolution in a morbidostat continuous culturing device with deep genomic sequencing of population samples collected in time series. This approach was applied to the experimental evolution of six populations of *Escherichia coli* BW25113 towards acquiring resistance to triclosan (TCS), an antibacterial agent in various consumer products. This study revealed the rapid emergence and expansion (up to 100% in each culture within 4 days) of missense mutations in the *fabI* gene, encoding enoyl-acyl carrier protein reductase, the known TCS molecular target. A follow-up analysis of isolated clones showed that distinct amino acid substitutions increased the drug IC₉₀ in a 3–16-fold range, reflecting their proximity to the TCS-binding site. In contrast to other antibiotics, efflux-upregulating mutations occurred only rarely and with low abundance. Mutations in several other genes were detected at an earlier stage of evolution. Most notably, three distinct amino acid substitutions were mapped in the C-terminal periplasmic domain of CadC protein, an acid stress-responsive transcriptional regulator. While these mutations do not confer robust TCS resistance, they appear to play a certain, yet unknown, role in adaptation to relatively low drug pressure. Overall, the observed evolutionary trajectories suggest that the FabI enzyme is the sole target of TCS (at least up to the ~50 μm level), and amino acid substitutions in the TCS-binding site represent the main mechanism of robust TCS resistance in *E. coli*. This model study illustrates the potential utility of the established morbidostat-based approach for uncovering resistance mechanisms and target identification for novel drug candidates with yet unknown mechanisms of action.

DATA SUMMARY

Illumina sequencing data in FastQ format have been deposited at the National Center for Biotechnology Information (NCBI) Sequence Read Archive [1] and can be downloaded from the NCBI BioProject database using accession number PRJNA472810 (<https://www.ncbi.nlm.nih.gov/bioproject/PRJNA472810>). The supplementary data (text, figures and tables) are available on Figshare (<https://doi.org/10.6084/m9.figshare.13076264>). A detailed description of the morbidostat implementation, the scripts for NGS data processing and the tool for calling IS element reallocation (iJump) can be found in the following GitHub repositories: https://github.com/sleyn/morbidostat_construction, https://github.com/sleyn/Triclosan_EE_paper and <https://github.com/sleyn/ijump>, respectively.

INTRODUCTION

Antibiotic resistance is a major threat to public health. According to US and European Centers for Disease Control and Prevention reports, infections by drug-resistant bacteria cause more than 30000 deaths per year [2, 3]. At the same time, the current pace of development and regulatory approval of new antibiotics is too slow to curb the spread of acquired multidrug resistance. Thus, of 51 antibiotics

Received 24 October 2020; Accepted 08 March 2021; Published 04 May 2021

Author affiliations: ¹Sanford Burnham Prebys Medical Discovery Institute, La Jolla, CA, USA; ²Evolugate, Gainesville, FL, USA; ³Roche Pharma Research and Early Development, Immunology, Infectious Diseases and Ophthalmology, Roche Innovation Center, Basel, Switzerland; ⁴Roche Pharma Research and Early Development, Pharmaceutical Sciences, Roche Innovation Center, Basel, Switzerland.

*Correspondence: Andrei L. Osterman, osterman@sbpdiscovery.org

Keywords: experimental evolution; morbidostat; antibiotic resistance; triclosan; *Escherichia coli*.

Abbreviations: MIC, minimum inhibitory concentration; TCS, triclosan.

Data statement: All supporting data, code and protocols have been provided within the article or through supplementary data files. Seven supplementary tables and six supplementary figures are available with the online version of this article.

000553 © 2021 The Authors



This is an open-access article distributed under the terms of the Creative Commons Attribution NonCommercial License.

and 11 biologics counted as being in development by the World Health Organization in 2017, only 10 are expected to be approved within the following 5 years [4]. Knowledge of the dynamics and mechanisms of acquired drug resistance across a range of target bacterial pathogens is one of the bottlenecks in the development and approval of new therapies. Historically, these features of new drug candidates have been addressed at a late stage of development, mostly because the traditional methodology of studying acquired resistance (via serial dilutions) is slow and labour-intensive [5]. The recent introduction of continuous culturing methodologies combined with highly efficient genome sequencing is expected to change the traditional drug discovery paradigm. It will enable the inclusion of 'resistibility' profiling at an earlier stage of testing and triaging drug candidates, on a par with conventional efficacy and safety testing. More efficient methods or experimental evolution-based drug resistance studies are also required to accelerate the identification of molecular targets of novel phenotypically selected antibacterial agents with unknown mechanisms of action.

Realization of the advantages of automated (computer-controlled) continuous culturing over manual serial dilution methods of experimental evolution [6] was enabled by the recently enhanced accessibility of 3D printing technology and programmable microcontrollers (such as Arduino and Raspberry Pi). One of the rapidly emerging custom-built continuous culturing devices [7–10], termed 'morbidostat', is a modification of the chemostat in which, instead of nutrient supply, the culture density is controlled by selective drug pressure [11, 12]. This approach enables gradual genetic adaptation of evolving bacterial populations to higher concentrations of an antibiotic and generally recapitulates the knowledge of resistance mechanisms from previous studies [11, 13, 14].

Among recently reported continuous culturing devices, eVOLVER [9] and omnistat [7] provide technologically sophisticated multi-purpose platforms supporting a broad range of microbial evolutionary experiments in chemostat,

Impact Statement

The current article describes the application of a morbidostat-based experimental evolution workflow for studying the dynamics and mechanisms of acquired antibiotic resistance, which is critical for the development and optimization of antimicrobial therapies. The established workflow enables accelerated studies of antimicrobial resistance via continuous culturing of target bacteria under automatically adjustable drug pressure combined with monitoring of the dynamics of mutation accumulation via deep sequencing of evolving bacterial populations in time series. We report the validation of this workflow in a model system of *Escherichia coli* evolving resistance to a common biocide triclosan (TCS), which revealed distinct evolutionary trajectories in six parallel reactors converging to a series of amino acid substitutions in the active site of enoyl-acyl carrier protein reductase FabI, the known TCS target. The practical significance of this work lies in the detailed description of the hardware and software components of a ready-to-implement workflow enabling antibiotic resistance studies for novel drug candidates.

turbidostat and morbidostat modes. The key feature of the eVOLVER platform is the capability for highly parallel processing of multiple samples over a variety of individually controlled experimental conditions. By the addition of specialized circuit boards and microfluidics, it can be customized to implement a morbidostat evolutionary mode. The omnistat platform features a simpler approach to automated liquid handling by bundling together a number of commercially available laboratory instruments. Our implementation of the morbidostat-based workflow (Fig. 1) included the engineering of a simple and robust device that uses inexpensive commercially available components, does not require sophisticated

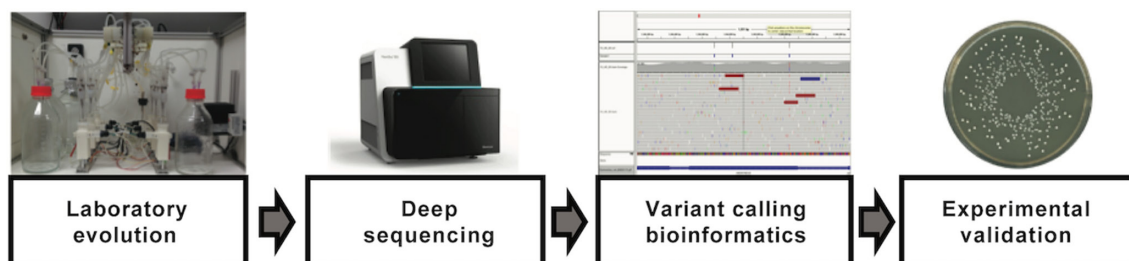


Fig. 1. The experimental evolution of antibiotic resistance workflow includes four main stages. (1) Bacterial populations are evolving under increasing selective drug pressure in six parallel reactors of the morbidostat, a continuous culturing device. Time series of samples are collected from each reactor. (2) Total genomic DNA from each sample is sequenced with high coverage to obtain quantitative representation of low- and high-frequency sequence variants in bacterial populations at every time point. (3) Possible resistance mechanisms are deduced from the dynamics of observed mutations. (4) Follow-up experiments aimed to test bioinformatic predictions and elucidate genotype-to-phenotype associations include verification of identified mutations and measurement of the extent of acquired resistance (MIC fold change) in selected representative clones.

robotics, and allows Arduino-based programmable process control and data acquisition (Fig. 2). Our current morbidostat design supports parallel evolution in six 20 ml reactors (glass tubes). It has a minimal number of parts requiring low-resolution 3D printing, and it may be seamlessly replicated in any research laboratory based on the detailed hardware and software description provided on GitHub (https://github.com/sleyn/morbidostat_construction).

At the end of the first stage of the workflow, a selective outgrowth in the morbidostat (Fig. 1), increased antibiotic resistance is tested experimentally in collected microbial population samples (one–two samples per day until maximum resistance is reached, typically within 3 to 8 days). At the next stage, total genomic DNA isolated from these samples is used for the preparation of non-amplified genomic libraries and deep sequencing (up to 1000× genomic coverage). Primary data processing using an assembled computational pipeline (see the Methods section and https://github.com/sleyn/Triclosan_EE_paper) yields a list of identified mutations (SNVs, small indels, genomic rearrangements including ‘jumping’ of IS elements), along with their fractional representation (%) in each sample. Further filtration with chosen confidence criteria (thresholds) and downstream analysis of gene-by-gene distribution and dynamics of accumulation of mapped variants across all reactors and time points lead to tentative identification of genetic features associated with antibiotic resistance. The final stage of the workflow is aimed at experimental testing of inferred genotype-to-phenotype associations via mapping of mutations and determination of MIC values for selected individual clones.

Here we report the application of this workflow for the experimental evolution of triclosan (TCS) resistance in a model system of *Escherichia coli* BW25113. TCS is an antimicrobial agent (biocide) commonly used in a variety of consumer products for dental care, cosmetics and soaps [15]. Extensive, indiscriminate use of TCS has led to its accumulation in the environment, in some soil samples reaching levels comparable to its MIC for *E. coli* and other susceptible bacterial pathogens (e.g. *Acinetobacter baumannii* and *Staphylococcus aureus*) [16]. An observed spontaneous acquisition of TCS resistance by pathogenic bacteria not only jeopardizes the utility of this biocide, but it may also pave the way toward their cross-resistance to some clinical antibiotics [17, 18].

The mechanism of action of TCS was established via the isolation of resistant clones with missense mutations in the gene *fabI* [19]. This essential gene encodes NADH-dependent enoyl-[acyl carrier protein] reductase, which is involved in one of the four elongation steps in fatty acid synthesis in most bacteria. TCS acts as a *FabI* inhibitor [19, 20], forming a stable and catalytically inactive TCS–NAD⁺–*FabI* complex [21–23]. In all eukaryotes the function of enoyl-[ACP] reductase is performed by a non-homologous domain of a multi-domain fatty acid synthase, which makes *FabI* attractive as a highly selective antimicrobial drug target. In some Gram-positive bacteria (such as *Streptococcus pneumoniae*) the gene *fabI* is replaced by a non-homologous isofunctional gene *fabK*,

which explains their intrinsic TCS resistance [19, 24]. In addition to some amino acid substitutions in the *FabI* target (most notably of Phe203 in *ecFabI*), an acquired TCS resistance was reported to result from overexpression of the *fabI* gene [25] and deregulation of efflux transporters [26]. However, according to some reports, TCS may also act on additional yet unknown targets at higher concentrations of the drug [27, 28].

Therefore, one goal of our study was to assess all possible mechanisms of acquired TCS resistance via experimental evolution across a broad range of TCS concentrations, from sub-MIC (<1 μm) to the highest concentration achievable in aqueous media (50 μm). The observed convergent evolution trajectories unambiguously pointed to the *FabI* enzyme being the sole protein target of TCS. We have identified a broad range of resistance-conferring amino acid substitutions in *FabI* (including all of the previously reported mutations) as the only tractable mechanism of robust TCS resistance in *E. coli*. All identified substitutions are localized in the vicinity of the *FabI*–TCS binding site and confer different levels of acquired resistance, ranging from ~3 to 16× MIC. This model study also points to the potential utility of the established morbidostat-based approach for uncovering resistance mechanisms and identifying targets for novel drug candidates with as yet unknown mechanisms of action.

METHODS

Morbidostat design (Fig. 2)

We designed and assembled the first version of the morbidostat device used in this study based on the principles described by Toprak *et al.* [12]. A detailed description of a more advanced current version of hardware and accompanying software is available from GitHub (https://github.com/sleyn/morbidostat_construction). Briefly, the main components of the device (Fig. 2c) include: (i) 6×20 ml bioreactors – glass tubes with magnetic stir bars and cap assemblies containing air-tight needle ports for feeding dilution media, constant air flow, and displacement of excess liquid after dilution; (ii) glass tubes fixed by silicone rings in 3D-printed plastic housings containing a laser and a sensor diode for measuring turbidity; (iii) a mini air-pump, which provides constant aeration for growing cultures (through sterile filters) and enables liquid displacement from reactors (over a fixed level corresponding to a total volume of 20 ml); (iv) a thermoregulated heater and mini-fan, which control the temperature inside the morbidostat enclosure box; (v) two 2 l feed bottles controlled by 2 peristaltic pumps connected by sterile tubing to an assembly of 12 check valves (2 valves per reactor, each connected to 1 of the 2 pumps) providing the flow of media (with and without antibiotic); (vi) a 6-position magnetic stir plate, which enables mixing (upon dilution) and agitation. An Arduino microcontroller is programmed to control the main parameters of the run: (i) temperature; (ii) time between dilutions (cycle time, CT); (iii) selection of the volume delivered by pump 1 (medium without drug) or pump 2 (medium with drug) for each culture dilution, depending on the culture turbidity and growth rate in each tube. A user interface for parameter

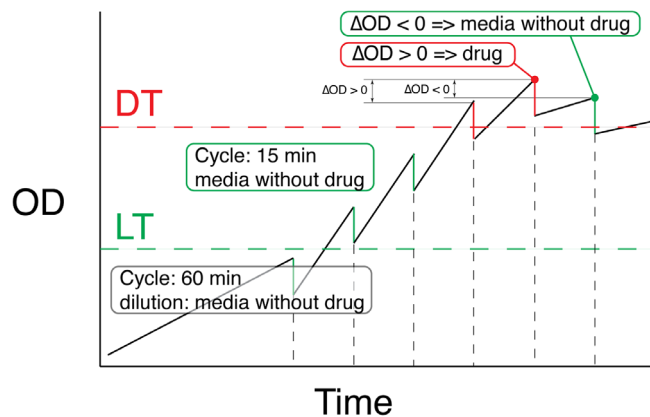
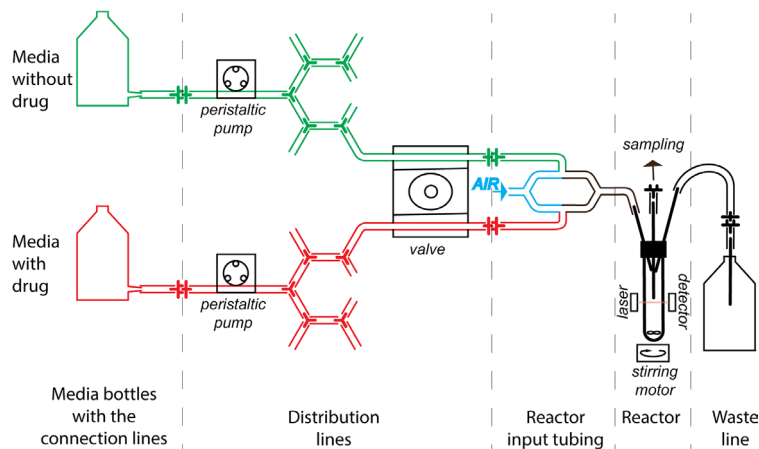
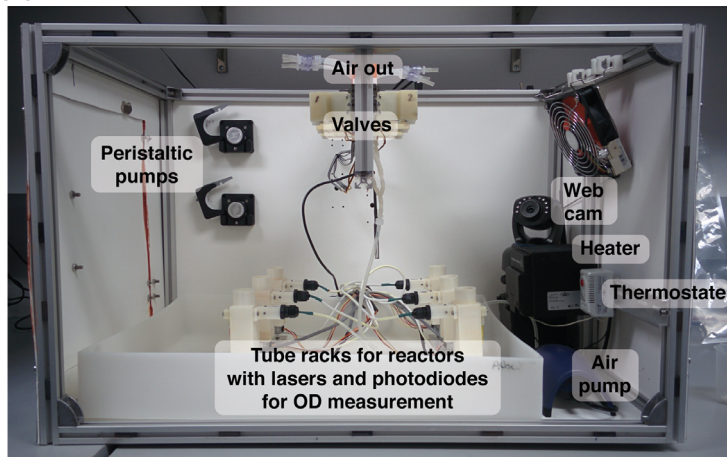
(a) Morbidostat logic**(b) Scheme****(c) Side view**

Fig. 2. Morbidostat approach implementation. (a) Morbidostat control logic: cultures with $OD <$ lower threshold (LT) are diluted with cycle time (CT)=60 min with the 'medium without drug' (pump 1). After growing to $OD >$ LT, CT is decreased to 15 min. At $OD >$ drug threshold (DT) the 'medium with drug' (pump 2) is added if the OD at the end of the current cycle is greater than at the end of the previous cycle. Otherwise the culture is diluted with medium without drug (pump 1). (b) General scheme of morbidostat. Two bottles: one containing medium without drug and the other containing medium with drug connected to two peristaltic pumps (pumps 1 and 2, respectively). Each pump is connected with six reactors. A valve on each tube controls media flow to individual reactors. Each reactor has three ports: (i) input for media and air, (ii) sampling port and (iii) waste line. The OD in each reactor is monitored by laser and photodiode. (c) Morbidostat device: side view with open box.

manipulation and real-time status display (including growth curves) is run on a PC using MegunoLink software (<https://www.megunolink.com/>).

The major differences between our implementation of morbidostat hardware and the originally published design [12] include (Fig. 2b):

- (i) using two pumps and a system of check valves to control the media flow instead of an array of multiple individual pumps, which allowed us to significantly simplify and increase robustness of the fluidics component;
- (ii) a permanent sterile-filtered air flow (disrupted only for short periods of time during media addition and mixing), which allows us to maintain constant volume (20 ml) in the reactor and create an air gap between media and culture; the latter allows us to avoid cross-contamination between reactors and input lines.

The encoded morbidostat logic (Fig. 2a) includes the following major steps:

- (1) an optical density at the end of the current cycle, before dilution (OD_1), is compared with two parameters: pre-defined drug threshold (DT) and optical density reached during the previous cycle (OD_0);
- (2) if $OD_1 \geq DT$ and $(OD_1 - OD_0) \geq 0$, the dilution is made by drug-containing medium (pump 2);
- (3) otherwise drug-free medium (pump 1) is added.

An additional step was introduced on top of the original morbidostat logic [12]. It operates with an additional pre-defined parameter, the lower threshold (LT) (see Fig. 2a), instructing the system to skip periodic dilutions (typically every 10–20 min for rapidly growing cultures such as *E. coli*) if $OD_1 < LT$ and instead perform hourly dilutions with drug-free medium. In the beginning of the run this feature allows all six cultures to reach the same minimal density ($OD_1 = LT$) prior to entering the active dilution mode. During the run, this ‘safe mode’ prevents a complete wash-out of the culture after an excessive dose of drug.

Parental strain

We used the *E. coli* BW25113 $\Delta uxaC::kan$ strain (JW3063) from the KEIO collection [29] as a starting point for the evolution of TCS resistance. The choice of this strain (instead of the wild-type BW25113) with a transposon-replaced nonessential gene (hexuronate transporter UxaC) was dictated by two considerations: (i) to take advantage of transposon-encoded kanamycin (Kan) resistance to guarantee sterility, and (ii) to leverage the KEIO collection of gene deletion mutants with the same genetic background for follow-up validation experiments. A total genomic DNA extract from the unevolved culture used to inoculate all six reactors of the morbidostat on day 1 was sequenced with mean coverage of 530×.

Evolutionary runs (Fig. 3)

On the first of the four consecutive evolutionary runs (day 1), growth in all six reactors of the morbidostat was started using the same inoculum of the chosen parental strain

[*E. coli* BW25113 $\Delta uxaC::kan$ strain (JW3063)]. This inoculum was obtained by propagation of the primary glycerol stock from the KEIO collection [29] in Luria-Bertani (LB) medium with 50 µg ml⁻¹ Kan and 2% DMSO. The overnight culture was diluted 100-fold, grown to $OD_{600} \sim 0.2$ and diluted 10-fold with the same medium, which was also used as drug-free (pump 1) medium for culture dilutions in the morbidostat over the course of the entire study. A drug-feeding (pump 2) medium had the same composition with 10 µm TCS (during day 1) or 50 µm TCS (days 2–4). In the following consecutive runs (days 2–4), glycerol stocks made from samples collected at the end of the previous run were used to inoculate respective reactors. A total of four one-day (continuous 24 h) runs were performed. After each run, six culture samples were collected; reactors and all feedlines were sterilized prior to starting the next run. The main parameters used in each run were: dilution volume V=2 ml (1/10 of total volume); LT=0.15; DT=0.4; CT=15 min. In addition to preparing glycerol stocks that were used for inoculation, MIC analysis, and later isolation of individual clones, a portion of each collected sample was used to prepare and freeze cell pellets for genomic DNA extraction.

Whole-genome sequencing (WGS)

Genomic DNA from the starting culture and 24 samples of evolving bacterial populations in time series (6 reactors × 4 days) was extracted from cell pellets with the Sigma Aldrich GenElute Bacterial Genomic DNA kit (NA2110). Sequencing libraries were prepared with the Illumina TruSeq DNA PCR-Free High Throughput Library Prep kit (#20015963) according to the manufacturer’s instructions. DNA was sequenced with the Illumina NextSeq 500 using 2×150 reads to reach up to 500–1000-fold genomic coverage in each sample (see Table S1, available in the online version of this article, for data quality and statistics). Reads were cleaned from adapter sequences, poly-G sequences and were trimmed by Phred base quality score with the Trimmomatic [30] (with ‘SLIDINGWINDOW:4:15 HEADCROP:10 CROP:145 MINLEN:65’ parameters). Cleaned reads were mapped onto an *E. coli* BW25113 genome downloaded from the PATRIC database (genome ID 679895.18) [31] with the BWA aligner [32] (using the ‘-M’ parameter). Alignments were corrected with lofreq viterbi [33] (using ‘-keepflags’ parameter). Quality scores were recalibrated with GATK BaseRecalibrator [34]. Sequencing data in fastq format have been deposited at the National Center for Biotechnology Information (NCBI) Sequence Read Archive (SRA), BioProject PRJNA472810.

Variant calling and downstream bioinformatics analysis

Variant calling was performed using lofreq [33] (with the ‘--call-indels’ parameter). The scripts are available in the https://github.com/sleyn/Triclosan_EE_paper GitHub folder. Variants in repeat regions were filtered out. The repeat regions were identified via self-alignment of the *E. coli* BW25113 genome using NUCmer [35] according to the ‘Identifying repeats’ section of the MUMmer manual (<http://mummer.sourceforge.net/manual/>) and filtered out. To eliminate

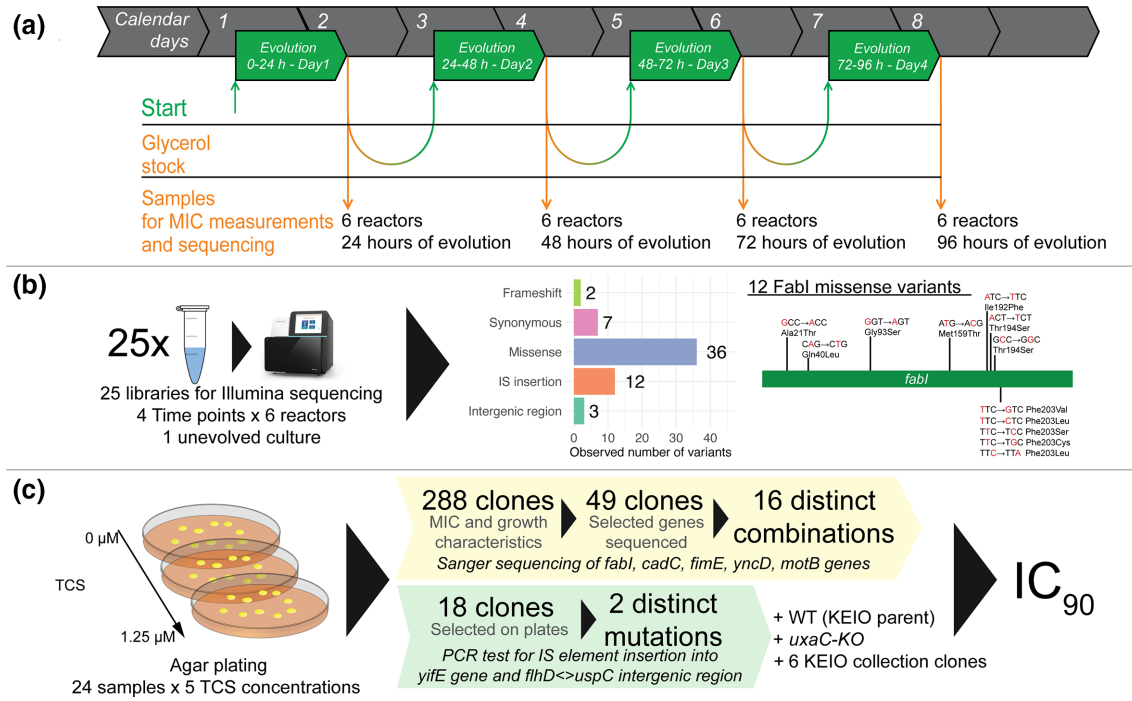


Fig. 3. Experimental evolution of TCS resistance. (a) Six parallel reactors were inoculated from a single stock of *E. coli* BW25113 ΔuxuC::kan strain from the KEIO collection [29] and cultured in the morbidostat at 37 °C in four 24 h daily cycles (a-d). By the end of each daily cycle, the cultures were collected and split between cell pellets (for DNA extraction) and glycerol stocks used for inoculation of the next cycle. IC₉₀ was measured in collected samples of evolving bacterial populations to confirm the evolution of TCS resistance. (b) Total genomic DNA was purified from 25 samples [unevolved inoculum + (6 reactors × 4 daily cycles)] and used for Illumina sequencing. After primary data processing and variant calling, a total of 60 variants were identified and analysed for evolutionary dynamics and mechanistic implications. The mutations in enoyl-acyl carrier protein reductase *fabl* are shown as codons with mutated nucleotide and amino acid mutations. (c) For a set of 67 (49+18) isolated clones, 20 distinct variants (single, double and triple mutants) were mapped by PCR amplification/Sanger sequencing of selected loci. *E. coli* BW25113 (KEIO collection parent strain), *E. coli* BW25113 ΔuxuC::kan (parent strain for evolution runs) and 6 KEIO collection isolates (ΔcadC::kan, ΔcadA::kan, ΔmotB::kan, ΔyncD::kan, ΔlysP::kan, ΔcadB::kan) were added and IC₉₀ values for TCS were determined using the growth curve method.

sequencing biases manifest in unusual enrichment of low-frequency A→C and T→G variants, we applied additional filters to the lofreq output (see Methods S1). Structural variants were further analysed using the Breseq pipeline [36] in ‘population’ mode. To assess IS element rearrangements in populations, we have developed a new iJump tool (a description and the code are available on <https://github.com/sleyn/ijump>) [37]. The list of IS elements for tracking their rearrangements was created by using BLASTN of the reference genome against the ISfinder database [38]. The IS element BLAST hits were filtered to keep ones with e-values <10⁻³⁰ and the highest bitscore among overlapping hits (see Table S2). We kept iJump insertion predictions that reached at least 1% frequency in any reactor after summarizing frequencies estimated for all copies of IS elements. iJump predictions were inspected manually in BAM alignments with samtools [39] and Tablet [40]. To assess evolutionary dynamics, Muller plots were constructed for a subset of predominant mutations (selected from the complete list of observed confident structural variants provided in Table S3) and their combinations were tentatively deduced from synchronous patterns of variant frequencies. The ‘MullerPlot’ R package [41] was used for plot visualization. Initial plots

were further adjusted based on the analysis of mutations in isolated individual clones.

Selection and characterization of individual clones

We used LB agar plates with a range of TCS concentrations (from 0 to 1.25 µM) to perform colony-forming unit (c.f.u.) analysis of 24 collected samples (6 reactors × 4 time points) of evolving populations in comparison with the unevolved starting culture of the *E. coli* BW25113 ΔuxuC::kan strain (see Fig. S2). From this initial screening, a total of 288 clones were selected for the initial assessment of MIC values by a microplate growth curve method using endpoint growth/no-growth measurements at 12 and 24 h (see below) (Table S6). Based on the diversity of MIC values and the representation of distinct sequence variants across all reactors and time points, 49 clones were ultimately selected for mapping of candidate mutations. This was achieved using PCR amplification and Sanger sequencing of selected regions in the *E. coli* genome (covering genes *fabl*, *cadC*, *fimE*, *yncD*, *motB*, *rpoA*) that contained the most prominent mutations. The obtained PCR products were sequenced by Eton Bioscience,

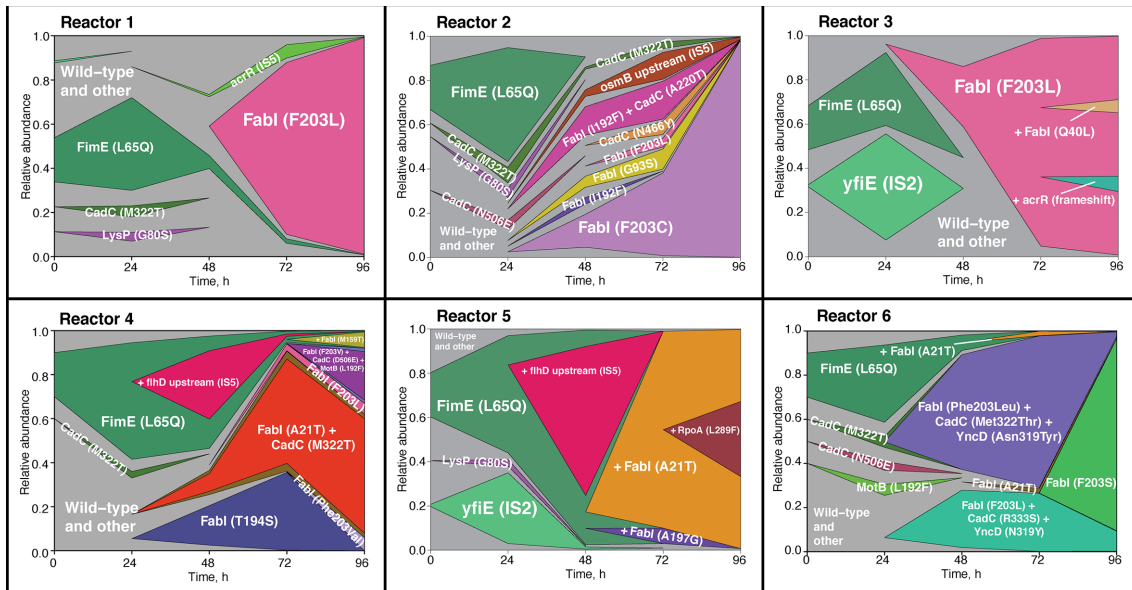


Fig. 4. Muller plots of *E. coli* evolution under triclosan stress in six reactors. Colours indicate various phenotypes. The labels on plot indicate emerged mutations. If a label begins with '+', then a mutation is emerging, with the other mutation in the background.

Inc. (<https://www.etonbio.com/>). Insertions of IS elements in the *yifE* gene and the *flhD-uspC* intergenic region were tested by comparing the size of the PCR products from additionally selected clones with the wild-type PCR product. The 18 clones for IS element analysis were selected separately from previously described samples; these clones were sourced from reactor 3 at 24 h ($n=8$) and reactor 5 at 48 h ($n=10$).

MIC determination (IC_{50} and IC_{90})

The acquired TCS resistance of selected clones was measured using a serial dilution method. Clones were grown on LB/Kan (50 μ g ml $^{-1}$) agar plates. Colonies were resuspended in 1 ml of MHB/Kan solution and 5–10 μ l of suspension was then incubated in 1 ml of MHB/Kan and 2% DMSO in 96-well plates with a range of increasing TCS concentrations. For the lower range (closer to the IC_{90} of the unevolved parental strain=0.65 μ m) the final concentrations of TCS were: 0, 0.3125, 0.625, 1.25, 2.5, 5, 10 and 20 μ m. For 22 h, the OD of each sample at each concentration was measured at 600 nm wavelength by a BioTek ELx808 plate reader at 37 °C. For each well, the area under the growth curve (AUC) was calculated using the 'growthcurver' R package [42]. The IC_{90} values were calculated from the AUC-TCS concentration data (in independently grown duplicates) using the 'drc' R package and a curve-fitting procedure [43]. We used the LL4 model for curve-fitting. The same method was used to estimate changes in the apparent values of MIC in evolving populations (see Fig. S1), except that diluted glycerol stocks of collected samples, instead of individual colonies, were used to inoculate the microtitre plates.

RESULTS

Populational dynamics of experimental evolution in the morbidostat

Pre-existing mutations in the unevolved population

Of the 10 pre-existing variants (listed in Table S4) revealed by comparison with the published genomic sequence of *E. coli* BW25113 (RefSeq assembly GCF_000750555.1), only 2 mutations affected the whole population (~100% frequency): the G470S missense variant in the *nrr* gene encoding bifunctional NAD(P)H-hydrate repair enzyme and the disruption of *lrhA* gene (encoding a transcriptional regulator) mediated by IS2 mobile element.

Among other variants represented in the initial population (within the 1–20% frequency range), two variants displayed interesting dynamics during the course of experimental evolution (Fig. 4). First, a L65Q missense mutation in gene *fimE* encoding regulatory recombinase of the type I fimbriae formation expanded from 20 up to ~50% of populations during day 1 in all six reactors. This expansion was followed by elimination of the *FimE:L65Q* variant at a later stage in all reactors except R4, where it remained at the level of ~10%, and R5, where the main resistance-driving variant *FabI:A21T* emerged on *FimE:L65Q* background and extended to cover the entire bacterial population. Notably, the population representation of the *FimE:L65Q* variant showed good correlation with the frequency of the ON vs OFF position of the *fim* switch (Pearson correlation coefficient $r=0.92$, see Fig. S3). This observation suggests that *FimE:L65Q* likely has a lower recombinase activity, which controls the regulation of type I fimbriae expression via on-to-off recombination of the *fim* switch region [44]. This conjecture is consistent with

the predicted localization of the L65 residue near the active site in a FimE 3D model (Fig. S4). Second, a low-frequency (~1%) disruption of the *yifE* (*maoP*) gene by the IS2 mobile element also expanded up to 31 and 48% of populations during day 1 in two out of six reactors. The remaining low-medium frequency pre-existing variants quickly disappeared from populations by day 2–3 in all or most of the reactors, along with the emergence and expansion of TCS-resistant FabI mutants.

Dynamics of TCS resistance and mutations in evolving bacterial populations

The dynamics and extent of TCS resistance acquired over the course of experimental evolution (days 1–4) were estimated using two approaches. First, the apparent ‘population-wide’ IC₉₀ was assessed using a standard growth curve method without isolation of individual clones. The estimated IC₉₀ showed a general trend, increasing from 2- to 4-fold in days 1–2 up to 10–20-fold by day 4 (Figs 3 and S1). Second, we performed c.f.u. analysis on agar plates over a range of TCS concentrations. This analysis revealed a gradual increase in the frequency of clones growing at TCS concentrations above the MIC of the unevolved strain (Fig. S2). Thus, in most reactors, between days 2 and 4, the extent of populational resistance increased from 12–15% of clones growing at the highest TCS concentration, corresponding to 1× MIC, up to 40–70% growing at 4–8× MIC. Up to 300 clones representing different time points and extents of evolved TCS resistance across all 6 reactors were picked for further analysis.

Following verification of gradual acquisition of drug resistance, total genomic DNA from all 24 collected populational samples was sequenced with a mean coverage of ~1000× (sd ~300×) (see Table S1). Upon primary data analysis, variant calling and filtration, we identified 60 distinct sequence variants that appeared in at least 1 reactor (see Table S3). Among them, were 36 missense and 7 synonymous mutations, 2 frameshifts, and 3 intergenic region mutations and small indels. In addition, 12 IS element insertion events were mapped using a newly developed iJump programme.

A tentative reconstruction of the dynamics of the appearance and disappearance of the main sequence variants created from deconvolution of populational sequencing data (Table S3), illustrated here by Muller plots (Fig. 4), revealed some notable trends. At an early stage of experimental evolution (days 1–2, up to 48 h), we only see a limited accumulation of new mutations. As already mentioned, the predominant adaptation processes included expansion within day 1 of the two pre-existing variants, FimE:L65Q (in all reactors) and *yifE*:IS2 (in reactors 3 and 5). While in most cases, these variants were outcompeted and eliminated from populations by day 3, in one reactor (R5), the FimE:L65Q variant expanded to 100% and was sustained over the entire course of evolution due to the emergence of additional FabI mutations on the FimE:L65Q background.

Several low-frequency missense mutations (1–7%) in genes *cadC*, *lysP* and *motB* that appeared within day 1 in at least one

reactor (up to four reactors in the case of the CadC:M322T variant) either disappear by day 2 or combine with one of the emerging FabI mutations and expand at a later stage. In most reactors at an early stage (days 1–2), FabI mutations do not emerge at all (as in R1 and R5) or accumulate at a relatively low level (≤30%, as in R2, R3 and R4). However, in R6, a FabI:F203L variant reaches ~80% of population at day 2 as a triple mutant combined with missense mutations in CadC and YncD (see Fig. 4, Table S3). The observed faster accumulation of FabI in R6 is consistent with more rapid acquisition of robust TCS resistance at an earlier stage (day 2) of evolution (see Figs S1 and S2). The initial tentative assignment of double (and some triple) mutants that become predominant at a later stage (starting day 3) in most reactors (except R1), was based on parsimonious analysis of parallel trends in the frequency of mutations (from Table S3). However, most of the assignments shown in Fig. 4 were later verified by sequencing of selected individual clones (see Table 1).

Importantly, the dynamics of the appearance and expansion of double mutants allow us to confidently reconstruct some of the evolutionary trajectories. These dynamics also permit us to distinguish mutations that could only have emerged in the course of evolution, as opposed to those resulting from selective propagation of pre-existing micro-SNPs. Thus, in addition to the example of R6 outlined above, another mutation, FabI:A21T, emerged in R4 at day 2 in the background of a CadC:M322T variant (initially detected in day 1 without any FabI mutations). Starting at day 2, both mutations expanded in parallel from ~10% ion day 2 up to >50% on day 4 (see Fig. 4, Table S3). The inferred co-occurrence of both mutations in one clone was later verified directly (Table 1).]

Nevertheless, the most important and obvious trend is the evolution of robust TCS resistance via a range of alternative amino acid substitutions in the known TCS target, the enoyl-[ACP]-reductase FabI target, as a single general mechanism. Despite different observed dynamics and a diverse array of specific mutations and combinations thereof, 97–99% of bacterial populations in all reactors at day 4 contained at least one FabI variant (most commonly F203L or F203C). The emergence of a FabI:Q40L variant in the background of the dominant FabI:F203L mutant on day 4 in R3 was inferred from population sequencing data (Fig. 4), but the respective clone was not isolated due to low frequency (~6%).

Mechanistically relevant variants

Overall, we identified 12 missense variants in 8 positions in the gene *fabI* that are distinct at a nucleotide level, resulting in 10 amino acid substitutions. All of the respective amino acid residues are located in the vicinity of the TCS-binding site in the known 3D structure of the FabI-NADH-TCS complex (Fig. 5) [23]. Five out of 12 variants are substitutions at FabI:F203 (2 versions of F203L; F203C; F203V; and F203S). Notably, these variants are predominant at day 4 in nearly all reactors except R5, which is dominated by FabI:A21T. However, the A21T mutation of FabI is the second most frequent among all FabI variants and only reaches 99% in the reactor lacking any FabI:F203 variants (R5). This observation is consistent with a

Table 1. IC₉₀ and 95% confidence Interval (CI) values for clones isolated in this study (bold) and selected KO strains from the KEIO collection (gene ID in parentheses). The variants are highlighted by distinct positions of FabI mutations and sorted in ascending order by IC₉₀ values. The colour in the second column shows the IC₉₀ gradient from low (green) to high (red)

| Evolved variants and KO strains | IC ₉₀ (μm) | CI | Fold change |
|--|-----------------------|------------|-------------|
| <i>I. Evolved FabI variants</i> | | | |
| FabI:T194S+CadC:M322T | 1.99 | 1.79–2.18 | 3 |
| FabI:T194S | 2.23 | 1.74–2.72 | 3 |
| FabI:I192F | 3.52 | 3.25–3.78 | 5 |
| FabI:A21T+CadC:M322T | 3.56 | 3.36–3.77 | 5 |
| FabI:A21T+FimE:L65Q | 4.1 | 3.70–4.51 | 6 |
| FabI:A21T | 4.12 | 3.76–4.48 | 6 |
| FabI:I192F+CadC:A220T | 4.52 | 4.31–4.74 | 7 |
| FabI:F203L | 4.85 | 4.48–5.22 | 7 |
| FabI:G93S | 5.63 | 5.23–6.03 | 8 |
| FabI:F203V+CadC:D506E+MotB:L192F | 6.17 | 5.63–6.70 | 9 |
| FabI:F203L+CadC:M322T+YncD:N319Y | 6.72 | 6.23–7.21 | 10 |
| FabI:F203C | 7.37 | 6.84–7.90 | 11 |
| FabI:M159T+FimE:L65Q | 8.65 | 7.83–9.48 | 13 |
| FabI:F203V | 9.48 | 8.58–10.39 | 14 |
| FabI:F203S | 10.65 | 9.96–11.35 | 16 |
| <i>II. Other evolved variants</i> | | | |
| yifE:IS2* | 0.63 | 0.58–0.69 | 0.9 |
| us_flhD<>us_uspC:IS5† | 0.70 | 0.62–0.77 | 1.1 |
| <i>III. Unevolved parental strain</i> | | | |
| uxaC-KO (JW3063)‡ | 0.65 | 0.62–0.67 | |
| uxaC-KO (JW3063) +FimE:L65Q‡ | 0.7 | 0.63–0.78 | |
| WT | 0.85 | 0.75–0.96 | |
| <i>IV. KO strains from KEIO collection</i> | | | |
| cadC-KO (JW4094) | 0.6 | 0.58–0.61 | 0.9 |
| cadA-KO (JW4092) | 0.73 | 0.70–0.75 | 1.1 |
| motB-KO (JW1878) | 0.8 | 0.78–0.83 | 1.2 |
| yncD-KO (JW1446) | 0.91 | 0.87–0.94 | 1.4 |
| lysP-KO (JW2143) | 0.98 | 0.95–1.01 | 1.5 |
| cadB-KO (JW4093) | 1.01 | 0.95–1.06 | 1.5 |

*Evolved clone with IS2 insertion in *yifE* gene of unknown function.

†Evolved clone with IS5 insertion in the intergenic region between genes *flhD* and *uspC*.

‡Two clones with SNP in gene *fimE* were isolated from the inoculum of the unevolved parental strain.

§Wild-type BW25113 strain (ATCC).

superior intrinsic resistance/fitness of FabI:F203 variants. Of note, a double mutant containing a RpoA:L289F variant in the FabI:A21T background emerges and expands up to ~1/3 of the population in R5 at day 4 (Fig. 4). This variant was not

characterized at the clonal level, but since no other mutations in RpoA (alpha subunit of DNA-directed RNA polymerase) or any other genes involved in DNA/RNA metabolism were detected, its impact on TCS resistance/fitness appears unlikely.

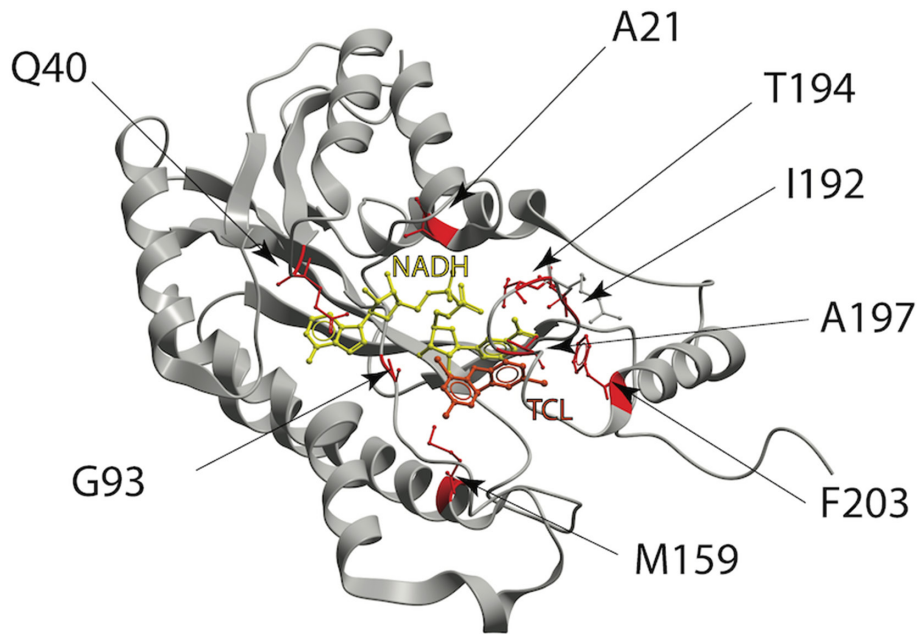


Fig. 5. Three-dimensional structure of FabI (PDB ID: 1QSG [23]) with NAD (yellow) and TCS (orange). Amino acid residues affected by mutations identified in this study are coloured red. For mutations where the IC₉₀ is known it is shown by extension lines in μm.

Beyond FabI target-based adaptation, only two low-frequency events disrupting the *acrR* gene, the known transcriptional repressor of the multidrug efflux transporter AcrAB [45], have a clear link to a possible mechanism of TCS resistance. An *acrR* frameshift mutant emerged at day 4 and reached 7% in the population of R3 on the background of the predominant FabI:F203L variant. The second variant with IS5 mobile element insertion in *acrR* gene reached maximum frequency (6%) at day 3 in R1, but was outcompeted by the FabI:F203L single mutant by day 4. None of these variants were characterized at the clonal level due to frequency, and their actual contribution to TCS resistance remains unknown.

Other evolved variants

As noted above, mutations in other genes reached appreciable levels either at an early stage and/or when combined with one of the FabI variants at a later stage of experimental evolution. Known functions of these genes do not point to any obvious links with TCS resistance. However, the observed multiple missense mutations in gene *cadC* point to a possible relevance of this integral membrane protein, a pH-sensing transcriptional activator of cadaverine pathway CadAB, for adaptation to a relatively low TCS pressure or another type of stress at the early stage of evolution. Notably, all five missense variants of CadC (A220T, M322T, R333S, N466Y and D506E) are found in the C-terminal signal-sensing domain of CadC 3D structure (PDB ID: 3LY7) [46]. Another observed early stage variant, LysP:G80S, observed in three reactors on day 1 (at ~3.5% frequency), affects lysine permease LysP, which is known to interact and negatively regulate CadC. Due to low frequencies of respective single mutants, none of these variants were characterized at the clonal level.

Another interesting variant, insertion of IS5 element upstream of the *fkhDC* operon, emerged and peaked in two reactors on day 3 (30% in R4 and ~70% in R5). This operon encoding transcriptional activators of the flagella biosynthesis pathway was disrupted by IS5 insertion at two positions: (i) -95/-99 interfering with LrhA (-89/-129) and OmpR (-101/-163) binding sites, and (ii) -315/-318 upstream of them (relative to the transcription start site according to Baker *et al.* [47]). These positions are known hotspots for IS element insertions leading to upregulation of flagellar and mobility genes in *E. coli* [47]. Notably, previously discussed IS2 insertions in the gene *yifE* also have a tentative association with the flagella pathway, as this gene is located upstream of *hdfR*, the regulator of flagellar master operon *fkhDC* [48]. Analysis of isolated clones representing both variants (see below) revealed no appreciable impact on TCS IC₉₀ (see Table 1), suggesting that a yet unknown adaptive role of these variants (if any) is not directly related to drug resistance.

Verification and characterization of individual evolved clones

A total of 49 clones representing the maximum diversity of TCS resistance (determined from preliminary screening of 288 clones, Fig. S2, Table S6) and anticipated mutations (deduced from evolutionary dynamics, Table S3) were selected for detailed characterization. This included accurate determination of TCS IC₉₀ and mapping of potential driver mutations by PCR amplification of the respective segments of the *cadC*, *fabI*, *yncD*, *motB*, *fimE* and *rpoA* genes. These results obtained for 15 evolved clones with mapped distinct mutations and 2 distinct sub-clones isolated from the

unevolved population of BW25113 $\Delta uxaC::kan$ strain (with and without FimE:L65Q variant) are provided in Table 1. In addition, two clones representing IS element insertions in the *yifE* gene and the *flhD-uspC* intergenic region were isolated from the respective samples, verified by PCR/Sanger sequencing and tested for TCS resistance. A panel of characterized clones covered nearly all of the FabI single mutant variants and some of the observed double and triple mutants. The observed IC_{90} values vary substantially in a range from ~2 up to >10 μm over the entire panel of 15 FabI variants (section I in Table 1). This corresponds to a fold change from 3 to 16 \times as compared to the averaged IC_{90} of the parental strain sub-clones of *E. coli* BW25113 $\Delta uxaC::kan$ with and without the FimE:L65Q variant (section III in Table 1). These variations depend on the position and specific amino acid substitution (as in the case of multiple FabI:F203 variants) but, with a few exceptions, show almost no dependence on the presence or absence of mutations in other genes. The observed variations in TCS resistance are generally consistent with the outcome of convergent evolution, which included the competition of distinct FabI variants within the same reactors. As already emphasized, most day 4 populations are dominated by the FabI:F203-driven variants that show the highest level of TCS resistance. Not surprisingly, at day 4 in R6, the FabI:F203S single mutant, which has the highest IC_{90} (10.7 μm), ultimately outcompeted a triple mutant (FabI:F203L+CadC:M322T+YncD:N319Y) with a somewhat lower IC_{90} (6.7 μm).

Although CadC single mutant variants were not isolated due to their low frequency, we used a series of strains from the KEIO collection [29] to assess the effect of individual gene knockouts in the *cad* pathway (genes *cadC*, *cadA*, *cadB*, *lysP*) on TCS resistance (Table 1). CadC is a transcriptional activator of lysine/cadaverine antiporter *cadB* and lysine decarboxylase *cadA* [49], and lysine transporter *lysP* is a posttranslational negative regulator of CadC [50]. Therefore, deletion of *cadC* might be expected to have a negative effect, similar to that of the deletion of *cadA* or *cadB*, and opposite to the effect of *lysP* deletion. However, the observed IC_{90} values were either nearly the same (for CadC-KO and CadA-KO) or only ~1.5-fold higher (for CadB-KO, LysP-KO) than for the isogenic control strain (*UxaC-KO*).

Cross-resistance between biocides and antibiotics is a concern for the overuse of TCS in consumer products, and exposure to biocides was found to decrease the susceptibility of *Salmonella* to multiple antibiotics, including broad-spectrum quinolones [51]. Since their presence did not increase TCS resistance directly, a series of CadC variants were examined for possible cross-resistance effects of such mutations. Five single FabI-mutant clones and seven double CadC-FabI mutant clones (with shared FabI mutations) were tested for resistance to various antibiotics (ampicillin, chloramphenicol, ciprofloxacin, erythromycin and tetracycline). All clones had the same MIC for each tested drug, exhibiting no cross-resistance trends with the presence or absence of CadC mutations.

DISCUSSION

In this study we have evaluated the morbidostat-based continuous culture method to study the evolution of antibiotic resistance. For this purpose, we have established an experimental evolution workflow (Fig. 1), which included engineering a morbidostat device based on a published conceptual design (Fig. 2) [12], and applied the workflow and device to study the evolution of TCS resistance in *E. coli* (Fig. 3). This analysis revealed a notable diversity of emerging mutant variants expanding and contracting in six parallel bacterial cultures and showing distinct evolutionary trajectories. All these trajectories converged within 4 days into a limited number of solutions (Fig. 4) sharing one general mechanism of robust TCS resistance (up to 16-fold increase in IC_{90}) driven by a range of adaptive amino acid substitutions in the vicinity of NAD/TCS-binding site of the known target enzyme enoyl-[ACP]-reductase FabI (Fig. 5). The 8 detected amino acid residues comprising a total of 12 distinct substitution variants included all 3 FabI positions (G93, M159 and F203) previously reported to confer robust TCS resistance [19, 24]. These three positions, most notably F203, featuring four distinct substitutions, are associated with FabI variants dominating bacterial populations at the latest stage of evolution and showing the highest extent of TCS resistance measured in isolated clones (Table 1). Other FabI variants identified only in this study (affecting A21, Q40, I192, T194 and A197 residues) were generally less competitive (except for a special case of A21T) and showed lower IC_{90} for TCS. This observation illustrates an advantage of the dynamic genomic profiling-based approach (over a more conventional clone isolation) for the detection of transient variants with lower drug resistance and/or fitness. Remarkably, most of these 'low-ranking' residues are located at the NAD side of the FabI-NAD-TCS complex (Fig. 5), and some of them (I192 and T194) were shown to form hydrogen bonds with NAD [23]. Therefore, it is tempting to hypothesize that the respective mutations are more likely to confer TCS resistance via shifting NAD position in the FabI active site, which may be a less efficient strategy than a direct interference with TCS binding. Indeed, the three 'high-ranking' residues (G93, M159 and F203) are located on the TCS side of the FabI-NAD-TCS complex and are known to form hydrophobic interactions with the TCS molecule [23].

Beyond FabI variants, we observed only two events potentially contributing to TCS resistance via upregulation of the *acrAB* efflux pump operon due to inactivation of the AcrR repressor. Both reached only a low frequency (6–7%) at the later stage (days 3–4) of experimental evolution. Although none of the respective clones were characterized, in previous studies, *acrAB* overexpression was shown to provide only a twofold increase in TCS-resistance [26]. These observations generally suggest that AcrAB-driven efflux upregulation provides a degree of resistance or fitness that is less competitive under selective conditions in the morbidostat.

Of the early stage events (Fig. 4, Table S3), several low-frequency missense mutations in the gene *cadC* (and one in *lysP*) appeared to be the most promising candidates for an

alternative mechanism of TCS resistance. This conjecture was based on the observed variety of independent, distinct and exclusively missense mutations that are all localized in the C-terminal periplasmic domain of the pH-sensing CadC transcriptional activator of the *cadBA* operon. Although the exact function and mechanism of action of CadC have not been fully elucidated, it has been implicated in acid stress response, which could provide a mechanistic basis for the adaptation to TCS-induced stress. However, a comparative characterization of the five pairs of isolated FabI single mutant variants with respective (FabI + CadC) double mutants failed to provide conclusive support for this hypothesis (see Table 1, Fig. S5). Therefore, at this point a mechanistic role of the observed *cadC* mutations in the evolution of TCS resistance (if any) remains unclear. Interestingly, a point mutation, CadC-Y504H, was implicated in the increased resistance of avian pathogenic *E. coli* to some plant-derived antibacterial agents, such as carvacrol [52].

The observed early-stage expansion of pre-existing variants (FimE:L65Q+YfiE:IS2), as well as the emergence of the (*flhD*-*uspC*:IS5) variant, point to a possible contribution of fimbriae and flagella biogenesis to TCS adaptation. This conjecture is consistent with previous reports on (i) activation of flagellar assembly genes in response to TCS [53, 54] and (ii) the contribution of fimbriae biosynthesis (genes *fimABCDEI*) to *E. coli* survival in the presence of TCS revealed by transposon mutagenesis [55]. However, none of the isolated clones representing these variants showed any improvement of TCS IC₉₀ (Table 1). Likewise, a double mutant (FabI:A21T+FimE:L65Q) variant showed the same level of TCS resistance as a respective single mutant FabI:A21T. Overall, the obtained clonal data did not provide support for the involvement of flagella or fimbriae pathways in the evolution of TCS resistance. The observed transient expansion of respective variants may be explained by the general adaptation to growth in the morbidostat or by compensation for the pre-existing IS2-disruption of the gene *lrhA* (Table S4), a master regulator of motility, chemotaxis, fimbriae and flagella biosynthesis genes [56].

In summary, in this study we have successfully used the established morbidostat-based workflow to assess the dynamics of experimental evolution and identify and verify a range of mutations driving acquired TCS resistance in *E. coli*. Despite the diversity of evolutionary trajectories and mutations across six parallel reactors, we have observed parallel evolution toward a single mechanism of robust TCS resistance (up to 16× increase of IC₉₀). This level of resistance is achieved by the substitution of at least one of several amino acid residues in the active site of FabI, the essential enzyme in fatty acid synthesis and the known TCS target. The established approach allowed us to detect all previously reported FabI mutations conferring TCS resistance and identify a broader set of previously undetected ones.

Overall, the obtained results provide a proof of concept and illustrate the potential advantages of the developed methodology for target identification (or verification) and the elucidation of yet unknown mechanisms of action and

resistance for established antibiotics and novel drug candidates. The prevalence of FabI mutations is in line with recent studies of bacterial isolates (human- and soil-associated) and metagenomes, where it was shown that mutations in FabI or substitutions to resistant analogues are the most abundant mechanisms for TCS resistance (see Table S7) [24, 57].

Funding information

This work was supported by an F. Hoffmann-La Roche Ltd pRED post-doctoral fellowship to S. L.

Acknowledgements

We want to thank Drs Pavel Pevzner (UCSD) and Sergey Nurk (St Petersburg State University) for consultations on computational data analysis, and Brian James and Kang Liu (at SBP Genomics Core Facility) for help with gDNA library preparation and Illumina sequencing.

Author contributions

Conceptualization: A. L. O., F. G. A. Data curation: S. A. L., J. E. Z. Formal analysis: S. A. L. Funding acquisition: A. L. O. Investigation: S. A. L., O. V. K., X. L., M. El., L. M., M. G., A. L. O. Methodology: S. A. L., J. E. Z., A. C., O. V. K., A. L. O. Project administration: A. L. O., S. A. L. Resources: A. L. O., S. A. L. Software: S. A. L., A. C. Supervision: A. L. O., F. G. A., M. Eb. Validation: S. A. L., A. L. O. Visualization: S. A. L. Writing – review and editing: J. E. Z., A. L. O., F. G. A., M. Eb.

Conflicts of interest

The authors declare that there are no conflicts of interest.

References

- Leinonen R, Sugawara H, Shumway M. International nucleotide sequence database C. the sequence read archive. *Nucleic Acids Res* 2011;39:D19–21.
- Cassini A, Höglberg LD, Plachouras D, Quattrocchi A, Hoxha A et al. Attributable deaths and disability-adjusted life-years caused by infections with antibiotic-resistant bacteria in the EU and the European economic area in 2015: a population-level modelling analysis. *Lancet Infect Dis* 2019;19:56–66.
- Centers for Disease Control and Prevention. Antibiotic resistance threats in the United States 2019.
- World Health Organization. Antibacterial agents in clinical development 2017.
- Barrick JE, Lenski RE. Genome dynamics during experimental evolution. *Nat Rev Genet* 2013;14:827–839.
- Gresham D, Dunham MJ. The enduring utility of continuous culturing in experimental evolution. *Genomics* 2014;104:399–405.
- Ekkers DM, Branco Dos Santos F, Mallon CA, Bruggeman F, van Doorn GS. The omnistat: a flexible continuous-culture system for prolonged experimental evolution. *Methods Ecol Evol* 2020;11:932–942.
- Gopalakrishnan V, Krishnan NP, McClure E, Pelesko J, Crozier D et al. A low-cost, open source, self-contained bacterial evolutionary biorEactor (eve). *bioRxiv* 2019;729434.
- Heins ZJ, Mancuso CP, Kiriakov S, Wong BG, Bashor CJ et al. Designing automated, high-throughput, continuous cell growth experiments using eVOLVER. *J Vis Exp* 2019 [Epub ahead of print 19 05 2019].
- Matteau D, Baby V, Pelletier S, Rodrigue S. A small-volume, low-cost, and versatile continuous culture device. *PLoS One* 2015;10:e0133384.
- Toprak E, Veres A, Michel J-B, Chait R, Hartl DL et al. Evolutionary paths to antibiotic resistance under dynamically sustained drug selection. *Nat Genet* 2011;44:101–105.
- Toprak E, Veres A, Yildiz S, Pedraza JM, Chait R et al. Building a morbidostat: an automated continuous-culture device for studying bacterial drug resistance under dynamically sustained drug inhibition. *Nat Protoc* 2013;8:555–567.
- Verhoeven E, Abdellati S, Nys P, Laumen J, De Baetselier I et al. Construction and optimization of a 'NG Morbidostat' - An automated

- continuous-culture device for studying the pathways towards antibiotic resistance in *Neisseria gonorrhoeae*. *F1000Res* 2019;8:560.
14. Döbelmann B, Willmann M, Steglich M, Bunk B, Nübel U et al. Rapid and consistent evolution of colistin resistance in extensively drug-resistant *Pseudomonas aeruginosa* during Morbidostat culture. *Antimicrob Agents Chemother* 2017;61 [Epub ahead of print 24 08 2017].
 15. Jones RD, Jampani HB, Newman JL, Lee AS. Triclosan: a review of effectiveness and safety in health care settings. *Am J Infect Control* 2000;28:184–196.
 16. Carey DE, McNamara PJ. The impact of triclosan on the spread of antibiotic resistance in the environment. *Front Microbiol* 2014;5:780.
 17. McNamara PJ, Levy SB. Triclosan: an instructive tale. *Antimicrob Agents Chemother* 2016;60:AAC.02105-16-6.
 18. Westfall C, Flores-Mireles AL, Robinson JI, Lynch AJL, Hultgren S et al. The widely used antimicrobial triclosan induces high levels of antibiotic tolerance *in vitro* and reduces antibiotic efficacy up to 100-fold *in vivo*. *Antimicrob Agents Chemother* 2019;63 [Epub ahead of print 25 04 2019].
 19. McMurry LM, Oethinger M, Levy SB. Triclosan targets lipid synthesis. *Nature* 1998;394:531–532.
 20. Heath RJ, Yu YT, Shapiro MA, Olson E, Rock CO. Broad spectrum antimicrobial biocides target the FabI component of fatty acid synthesis. *J Biol Chem* 1998;273:30316–30320.
 21. Heath RJ, Rubin JR, Holland DR, Zhang E, Snow ME et al. Mechanism of triclosan inhibition of bacterial fatty acid synthesis. *J Biol Chem* 1999;274:11110–11114.
 22. Roujeinikova A, Levy CW, Rowsell S, Sedelnikova S, Baker PJ et al. Crystallographic analysis of triclosan bound to enoyl reductase. *J Mol Biol* 1999;294:527–535.
 23. Stewart MJ, Parikh S, Xiao G, Tonge PJ, Kisker C. Structural basis and mechanism of enoyl reductase inhibition by triclosan. *J Mol Biol* 1999;290:859–865.
 24. Khan R, Kong HG, Jung Y-H, Choi J, Baek K-Y et al. Triclosan resistome from metagenome reveals diverse enoyl acyl carrier protein reductases and selective enrichment of triclosan resistance genes. *Sci Rep* 2016;6:32322.
 25. Grandgirard D, Furi L, Ciusa ML, Baldassarri L, Knight DR et al. Mutations upstream of fabI in triclosan resistant *Staphylococcus aureus* strains are associated with elevated fabI gene expression. *BMC Genomics* 2015;16:345.
 26. McMurry LM, Oethinger M, Levy SB. Overexpression of marA, soxS, or acrAB produces resistance to triclosan in laboratory and clinical strains of *Escherichia coli*. *FEMS Microbiol Lett* 1998;166:305–309.
 27. Villalain J, Mateo CR, Aranda FJ, Shapiro S, Micol V. Membranotropic effects of the antibacterial agent triclosan. *Arch Biochem Biophys* 2001;390:128–136.
 28. Escalada MG, Russell AD, Maillard J-Y, Ochs D. Triclosan-bacteria interactions: single or multiple target sites? *Lett Appl Microbiol* 2005;41:476–481.
 29. Baba T, Ara T, Hasegawa M, Takai Y, Okumura Y et al. Construction of *Escherichia coli* K-12 in-frame, single-gene knockout mutants: the Keio collection. *Mol Syst Biol* 2006;2:0008.
 30. Bolger AM, Lohse M, Usadel B. Trimmomatic: a flexible trimmer for illumina sequence data. *Bioinformatics* 2014;30:2114–2120.
 31. Wattam AR, Davis JJ, Assaf R, Boisvert S, Brettin T et al. Improvements to PATRIC, the all-bacterial bioinformatics database and analysis resource center. *Nucleic Acids Res* 2017;45:D535–D542.
 32. Li H, Durbin R. Fast and accurate short read alignment with Burrows-Wheeler transform. *Bioinformatics* 2009;25:1754–1760.
 33. Wilm A, Aw PPK, Bertrand D, Yeo GHT, Ong SH et al. LoFreq: a sequence-quality aware, ultra-sensitive variant caller for uncovering cell-population heterogeneity from high-throughput sequencing datasets. *Nucleic Acids Res* 2012;40:11189–11201.
 34. McKenna A, Hanna M, Banks E, Sivachenko A, Cibulskis K et al. The genome analysis toolkit: a MapReduce framework for analyzing next-generation DNA sequencing data. *Genome Res* 2010;20:1297–1303.
 35. Kurtz S, Phillippy A, Delcher AL, Smoot M, Shumway M et al. Versatile and open software for comparing large genomes. *Genome Biol* 2004;5:R12.
 36. Deatherage DE, Traverse CC, Wolf LN, Barrick JE. Detecting rare structural variation in evolving microbial populations from new sequence junctions using breseq. *Front Genet* 2014;5:468.
 37. Leyn SA. iJump: a fast tool for tracking bacterial mobile elements rearrangements in course of adaptive laboratory evolution [version 1; not peer reviewed]. DOI: <https://doi.org/10.7490/f1000research.1118098.1>. F1000Research, ISCB Comm J. 2020;9:799 (poster).
 38. Siguié P, Perochon J, Lestrade L, Mahillon J, Chandler M. ISfinder: the reference centre for bacterial insertion sequences. *Nucleic Acids Res* 2006;34:D32–D36.
 39. Li H, Handsaker B, Wysoker A, Fennell T, Ruan J et al. The sequence Alignment/Map format and SAMtools. *Bioinformatics* 2009;25:2078–2079.
 40. Milne I, Stephen G, Bayer M, Cock PJA, Pritchard L et al. Using tablet for visual exploration of second-generation sequencing data. *Brief Bioinform* 2013;14:193–202.
 41. Farahpour F, Saeedghalati M, Hoffmann D. MullerPlot: generates Muller Plot from Population/Abundance/Frequency dynamics data. R package version 012. 2016.
 42. Sprouffske K, Wagner A. Growthcurver: an R package for obtaining interpretable metrics from microbial growth curves. *BMC Bioinformatics* 2016;17:172.
 43. Ritz C, Baty F, Streibig JC, Gerhard D. Dose-Response analysis using R. *PLoS One* 2015;10:e0146021.
 44. Abraham JM, Freitag CS, Clements JR, Eisenstein BI. An invertible element of DNA controls phase variation of type 1 fimbriae of *Escherichia coli*. *Proc Natl Acad Sci U S A* 1985;82:5724–5727.
 45. Ma D, Alberti M, Lynch C, Nikaido H, Hearst JE. The local repressor AcrR plays a modulating role in the regulation of acrAB genes of *Escherichia coli* by global stress signals. *Mol Microbiol* 1996;19:101–112.
 46. Haneburger I, Fritz G, Jurkschat N, Tetsch L, Eichinger A et al. Deactivation of the *E. coli* pH stress sensor CadC by cadaverine. *J Mol Biol* 2012;424:15–27.
 47. Barker CS, Prüss BM, Matsumura P. Increased motility of *Escherichia coli* by insertion sequence element integration into the regulatory region of the flhD operon. *J Bacteriol* 2004;186:7529–7537.
 48. Ko M, Park C. H-NS-Dependent regulation of flagellar synthesis is mediated by a LysR family protein. *J Bacteriol* 2000;182:4670–4672.
 49. Kuper C, Jung K. CadC-mediated activation of the cadBA promoter in *Escherichia coli*. *J Mol Microbiol Biotechnol* 2005;10:26–39.
 50. Tetsch L, Koller C, Haneburger I, Jung K. The membrane-integrated transcriptional activator CadC of *Escherichia coli* senses lysine indirectly via the interaction with the lysine permease LysP. *Mol Microbiol* 2008;67:570–583.
 51. Webber MA, Whitehead RN, Mount M, Loman NJ, Pallen MJ et al. Parallel evolutionary pathways to antibiotic resistance selected by biocide exposure. *J Antimicrob Chemother* 2015;70:2241–2248.
 52. Al-Mnaser AA, Woodward MJ. Sub-lethal concentrations of phytochemicals (Carvacrol and Oregano) select for reduced susceptibility mutants of *Escherichia coli* O23:H52. *Pol J Microbiol* 2020;69:121–125.
 53. Lenahan M, Sheridan Áine, Morris D, Duffy G, Fanning S et al. Transcriptomic analysis of triclosan-susceptible and -tolerant *Escherichia coli* O157:H19 in response to triclosan exposure. *Microb Drug Resist* 2014;20:91–103.
 54. Bailey AM, Constantinidou C, Ivens A, Garvey MI, Webber MA et al. Exposure of *Escherichia coli* and *Salmonella enterica* serovar Typhimurium to triclosan induces a species-specific response, including drug detoxification. *J Antimicrob Chemother* 2009;64:973–985.
 55. Yasir M, Turner AK, Bastkowski S, Baker D, Page AJ et al. TraDIS-Xpress: a high-resolution whole-genome assay identifies novel mechanisms of triclosan action and resistance. *Genome Res* 2020;30:239–249.

56. Lehn D, Blumer C, Polen T, Wackwitz B, Wendisch VF et al. LrhA as a new transcriptional key regulator of flagella, motility and chemotaxis genes in *Escherichia coli*. *Mol Microbiol* 2002;45:521–532.
57. Khan R, Roy N, Choi K, Lee S-W. Distribution of triclosan-resistant genes in major pathogenic microorganisms revealed by metagenome and genome-wide analysis. *PLoS One* 2018;13:e0192277.

Five reasons to publish your next article with a Microbiology Society journal

1. The Microbiology Society is a not-for-profit organization.
2. We offer fast and rigorous peer review – average time to first decision is 4–6 weeks.
3. Our journals have a global readership with subscriptions held in research institutions around the world.
4. 80% of our authors rate our submission process as 'excellent' or 'very good'.
5. Your article will be published on an interactive journal platform with advanced metrics.

Find out more and submit your article at microbiologyresearch.org.